XVI International Conference on Computational Plasticity. Fundamentals and Applications
COMPLAS 2021
E. Oñate, D. Peric, M. Chiumenti and Eduardo de Souza Neto (Eds)

A COMPARISON OF FE ANALYSIS OF COLUMNS UTILIZING TWO STRESS STRAIN MATERIAL RELATIONS AND TWO DIFFERENT SOLVERS: ANSYS VS. SCIA ENGINEER

D. JINDRA*, J. KALA* AND Z. KALA*

* Institute of Structural Mechanics (STM) at the Faculty of Civil Engineering (FCE) of the
Brno University of Technology (BUT)
Campus Norte UPC, 08034 Barcelona, Spain
Veveří 331/95, 602 00 Brno, Czech Republic
e-mails: jindra.d@fce.vutbr.cz, kala.j@fce.vutbr.cz, kala.z@fce.vutbr.cz
web page: http://www.fce.vutbr.cz

Key words: Stainless Steel, Finite Element Numerical Model, CHS Columns buckling, ANSYS, SCIA Engineer.

Abstract. Paper presents results of the advanced numerical simulation processes of duplex stainless steel (EN grade 1.4462) circular hollow cross-section (CHS) columns in compression. Objective of the contribution is to compare the results of two different numerical finite element method (FEM) solvers: the ANSYS Classic technology and the solver utilized by the SCIA Engineer software. Normalized values of the ultimate axial load and the corresponding ultimate mid-height lateral deflection are statistically compared, considering the results of the experimental program, where 9 different column lengths of the 88.9×2.6 CHS have been analyzed. Secondary objective is to determine, whether a simplified linear elastic along with linear plastic (bilinear) stress-strain material relation is feasible for utilization in case of the numerical simulation of the slenderer duplex stainless steel column specimens, instead of more precise multilinear stress-strain relation defined in accordance with the behavior description proposed by Ramberg and Osgood.

1 INTRODUCTION

Duplex stainless steel as a material with high corrosion resistance has potential of utilization in many transportation structures (e.g. bridges, footbridges), as well as civil engineering applications, discussed e.g. by Baddoo [1]. This material is more recent in comparison with the much more commonly used carbon steel. For example, the first composite stainless steel bridge for vehicles in Europe was built on the island of Menorca, in Spain. The bridge was opened in Cala Galdana in June 2005 [2], and it is one of the firsts bridges worldwide, with a massive usage of the stainless steel material.

In comparison with the common carbon steel, the test data of stainless steel are much less numerous. Moreover, the stress-strain behavior of the stainless steel material is described by more rounded curve, with no significant yield point. Stainless steel has higher ductility, and the 0.2% proof stress value is adopted as the equivalent of the yield stress in conventional steel design. One of the objectives of this study (secondary objective) is to compare the difference between the ultimate load capacity determined by the numerical analysis for case of longer (and therefore slenderer) specimens, where a simplified bilinear stress-strain material relation has been utilized, with more detailed material behavior proposed by Ramberg and Osgood [3], later modified by Hill [4]. It is expected, that the significance of material nonlinearity is somehow smaller for slenderer columns (in comparison with shorter specimens), where rather geometrical nonlinearity has an important role.

Physical experiments of the duplex stainless steel (EN grade 1.4462) circular hollow sections presented in this study have been conducted by Buchanan et al [5], who have also conducted numerical simulations utilizing the Abaqus software [6]. Similar studies have been conducted by Gardner et al. [7] or again Buchanan et al. [8]. Arrayago et al. [9] have recently conducted a wide statistical study of stainless steel material parameters.

Main objective of this study is to conduct an advanced numerical simulation of the columns in compression in two different implicit numerical solvers: ANSYS Classic technology [10] and the FEM solver implemented in the SCIA Engineer software [11], and to statistically compare the results, in the matter of normalized values of the ultimate axial load and the corresponding ultimate mid-height lateral deflection).

2 EXPERIMENTAL TEST PROGRAM

Description of the experimental program is described in detail and documented in the study by Mr. Buchanan et al. [5] (p. 298 - 303). In this study, only the set of duplex stainless steel columns are considered, therefore the CHS 89×2.6 cross-section of 9 different structural lengths (400, 550, 750, 950, 1150, 1650, 2150, 2650 and 3080 mm) [5].

3 NUMERICAL FINITE ELEMENT MODEL

All 9 FE models of columns, which differed in structural lengths, cross-sectional parameters and global initial geometrical imperfections (based on Table 1) have been created in ANSYS Classic [10], as well as SCIA Engineer [11].

3.1 Model approach

In order to model the CHS columns, 4-nodal structural shell elements with 3 translational degrees of freedom (DoF) and 3 rotational DoF per node have been utilized. The stiffness of these elements consists of membrane and bending parts (Mindlin-Reissner theory). 3 integration points through the element thickness along with reduced integration with hourglass control (1 integration point in the plan view of the element) have been considered.

Geometrically, the utilized elements are rectangles. The maximal edge size of the elements in the longitudinal direction of the column is 8 mm, and 5 mm in the direction along the section circumference (tangentially). An example of the mesh is depicted in the Figure 1.

The circumferential nodes at both ends of the CHS column are connected with a single node located on the section axis by beam elements of high stiffness. The offset of this node is 77 mm, in accordance with the description of the experimental program (page 301 [5]). This boundary condition is implemented in order to model the pin-ended column.

For the bottom node (in ANSYS and SCIA as well), only the rotation along y axis is allowed in the global coordinate system (GCS), all the other 5 DoF are constrained.

Boundary condition of the upper node slightly differs between FE models in ANSYS and

SCIA, in order to utilize the possibilities of the SCIA Engineer software. In ANSYS, 2 rotational and 2 translational DoF are constrained. Rotation along y axis is allowed (to simulate the hinge), and the loading during the nonlinear analysis has been conducted by a prescribed displacement in the axial direction of the column (along the z axis of the GCS). In SCIA Engineer however, a nodal support (constrain) is required in order to define a corresponding displacement of that particular node. This would not be a problem utilizing a single node if no initial geometrical imperfections (based on the prior eigenvalue buckling analysis results) are desired to define. Therefore, 2 nodes, one close under the other (and connected by a stiff beam), have been utilized (Figure 1 left). The upper node (not constrained translationally in the z direction) was used for a loading force of the eigenvalue buckling (linear stability) analysis. The displacement load during the nonlinear analysis was conducted through the lower node. Even though this set-up has resulted in rather high and unrealistic value of the critical load factor (example in the Figure 2), the buckling shape of these linear stability analyses were feasibly utilized in order to define the initial geometrical imperfections.

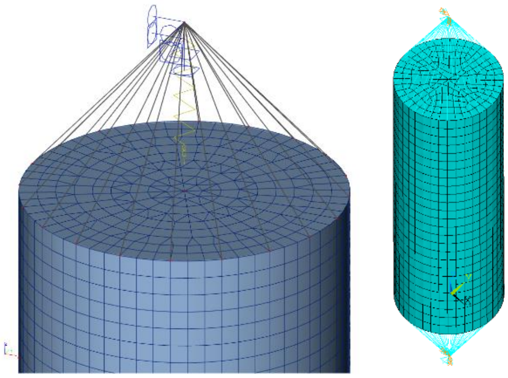

Figure 1: Mesh and boundary conditions; example of FE model from SCIA Engineer (left) and ANSYS (right)

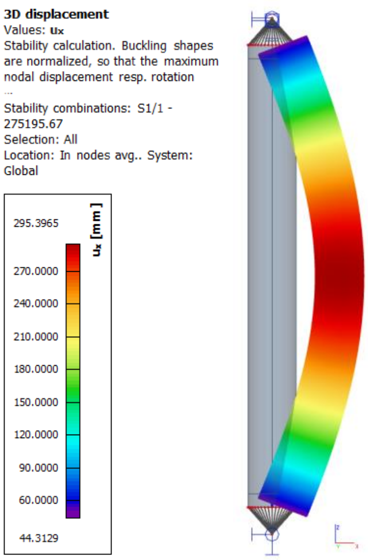

Figure 2: Result example of the eigenvalue buckling analysis (specimen 88.9×2.6-950-P); from SCIA Engineer

3.2 Geometry and initial geometrical imperfections

Geometrical parameters, D (cross-section outer diameter), t (wall thickness), L (effective structural length, including the additional knife edge lengths), and the initial global geometrical imperfection amplitudes ($\omega_0 + e_0$) have been considered in accordance with the measured values (Table 1 below, based on the data from the Table 7 from [5]).

Initial imperfections were incorporated into the numerical models utilizing the form of the lowest global buckling shape obtained either from prior modal analysis (ANSYS), or prior Eigenvalue buckling analysis (SCIA Engineer – example in Figure 2). The amplitudes of $\omega_0 + e_0$ were considered to simulate the initial imperfections and eccentricities. Local initial imperfections have been neglected, as in study [12]. More detailed modeling of imperfections using random fields [13] or combinations of eigenmodes [14] has not been applied.

Table 1: Measured geometric properties of the 89×2.6 CHS cross section set of the pin ended columns

Specimen	D [mm]	t [mm]	L [mm]	$L/(\omega_0 + e_0)$ [-]	$(\omega_0 + e_0)$ [mm]
88.9×2.6-400-P	88.63	2.37	403.90	824	0.490
88.9×2.6-550-P	88.63	2.35	553.83	1309	0.423
88.9×2.6-750-P	88.78	2.41	753.93	944	0.799
88.9×2.6-950-P	88.77	2.37	954.00	1075	0.887
88.9×2.6-1150-P	88.77	2.37	1154.00	1142	1.011
88.9×2.6-1650-P	88.63	2.35	1656.60	1022	1.621
88.9×2.6-2150-P	88.77	2.30	2152.80	716	3.007
88.9×2.6-2650-P	88.72	2.33	2653.40	993	2.672
88.9×2.6-3080-P	88.67	2.32	3082.50	1027	3.001

3.3 Material model

Two different definitions of the material model stress-strain dependence are considered, here referred as bilinear (simplified definition) and multilinear (more exact) material model. For the multilinear material model, the stress-strain behavior of the stainless steel material is defined by a relation proposed by Ramberg and Osgood [3], later modified by Hill [4]:

$$\varepsilon = \frac{\sigma}{E_0} + 0.002 \cdot \left(\frac{\sigma}{\sigma_{0.2}} \right)^n , \tag{1}$$

where σ and ε are stress and strain (nominal) respectively. E_0 is elastic modulus, $\sigma_{0.2}$ is the 0.2% proof stress, and n is a strain hardening exponent. For the strains above the $\sigma_{0.2}$ value, the stresses are overestimated [15]. A better agreement with the experimental data is achieved, when a 2-stage stress-strain relation recommended by Mirambell and Real [16] is used for the values above the 0.2% proof stress [15]. A modification of the second stage has been utilized, that is suitable for the compressive loadings in accordance with research by Gardner [7]:

$$\varepsilon = \frac{\sigma - \sigma_{0.2}}{E_{0.2}} + \left(0.008 - \frac{\sigma_{1.0} - \sigma_{0.2}}{E_{0.2}} \right) \cdot \left(\frac{\sigma - \sigma_{0.2}}{\sigma_{1.0} - \sigma_{0.2}} \right)^{n'_{0.2,1.0}} + \varepsilon_{t0.2} \Leftrightarrow \sigma > \sigma_{0.2} \tag{2}$$

where $\sigma_{1.0}$ is the 1.0% proof stress of the stainless steel, $n'_{0.2,1.0}$ is the second strain hardening exponent, and $E_{0.2}$ is tangent modulus (stiffness) at the 0.2% proof stress determined as:

$$E_{0.2} = \frac{E_0}{1 + 0.002 \cdot n \cdot E_0 / \sigma_{0.2}} \tag{3}$$

Multilinear material model with isotropic hardening (Mises plasticity) has been utilized for the numerical analyses. More detailed description of the stress-strain relation definition is to be read in author's previous study [17]. The nominal (engineering) stress-strain curves are required to be transferred into true (logarithmic) stress-strain dependences in order to be in match with the results of geometrically nonlinear numerical analyses:

$$\sigma_{true} = \sigma_{nom} \cdot (1 + \varepsilon_{nom}) \tag{4}$$

$$\varepsilon_{true} = ln(1 + \varepsilon_{nom}) \tag{5}$$

where σ_{nom} and ε_{nom} are engineering (nominal) stress and strains respectively (total mechanical values, elastic plus plastic). The ε_{nom} values have been input in negative values (for compression). However, a definition of a negative tangent of the stress-strain curve is not possible along with the isotropic hardening [10]. Therefore, the stress-strain relation has been considered as almost ideal plastic (with very little positive tangent) instead of softening after the peak stress value. A material model verification by one element uniaxial compressive test is depicted in the Figure 3 below (based on the parameter values from the Table 2).

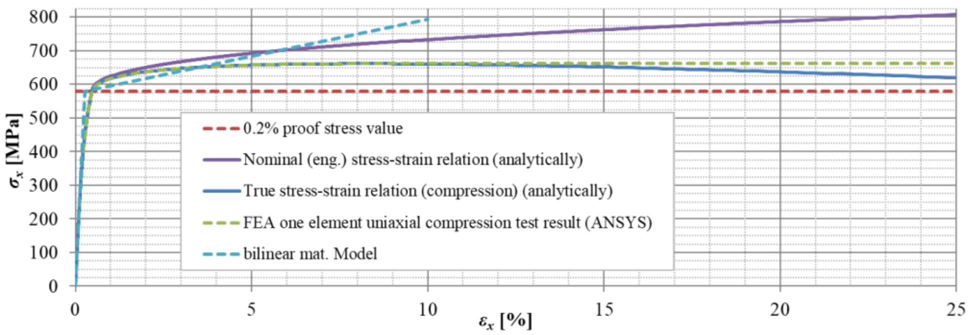

Figure 3: Material model verification by one element uniaxial compression test

Very small values of the membrane residual stresses have been observed in the cold-formed CHS members, and these are neglected [18]. The measured values of the material properties have been considered, therefore the through-thickness residual stresses are implicitly incorporated [19].

The material property values have been considered in accordance with the "stub column properties" as referred in the study by Mr. Buchanan et al. [5]. The values are averaged from the relevant available data (Table 4 from [5]), here summarized in the Table 2.

The simplified bilinear material definition only considers linear elastic material behavior up to the value of 0.2% proof stress $\sigma_{0.2}$. Afterwards, plastic hardening defined by a tangential modulus E_t is considered, with iteratively determined value (Table 2) in order to obtain the intersection of the bilinear and the multilinear material stress-strain curves at the value of strain approximately 5% (see Figure 3).

Table 2: Summary of the utilized material properties

Material model definition	E_0 [GPa]	$\sigma_{0.2}$ [MPa]	$\sigma_{1.0}$ [MPa]	n [-]	$n'_{0.2,1.0}$ [-]	σ_u [MPa]	$E_{0.2}$ [GPa]	E_t [GPa]
Multilinear	217.95	579.5	633.0	4.50	2.45	846.5	132.16	-
Bilinear	217.95	579.5	-	-	-	-	-	2.20

4 RESULTS

Monitored outputs of the numerical analyses are the axial load N, and the corresponding mid-height lateral deflection ω, and the force-displacement dependences are depicted in the Figure 4 – Figure 6. The ultimate values of the axial loads $N_{u,\#A}$ and $N_{u,\#S}$ based on the results of analyses in ANSYS and SCIA Engineer respectively, along with the corresponding ultimate mid-height lateral deflections $\omega_{u,\#A}$ and $\omega_{u,\#S}$ are documented in the Table 3. $N_{u,exp}$ and $\omega_{u,exp}$ are the experimental values of the corresponding monitored parameters [5].

Global slenderness $\bar{\lambda}$ and the cross-section class (cl.) provided in the Table 3 are determined in accordance with the EN 1993-1-4 [20], in dependence on the cross-sectional and material properties.

Statistical parameters (arithmetic average value, standard deviation and the coefficient of variation, CoV) of the processed sets, the normalized values of axial load $N_{u,\#}/N_{u,exp}$ and the normalized value of the mid-height lateral deflection $\omega_{u,\#}/\omega_{u,exp}$ are summarized in the Table 4 for both numerical model environments, ANSYS (#A) and SCIA Engineer (#S).

Table 3: Results of the finite element analyses of the 89×2.6 CHS pin ended columns

Specimen	$\bar{\lambda}$ [-]	*cl.*	$N_{u,\#A}$ [kN]	$\omega_{u,\#A}$ [mm]	$N_{u,\#S}$ [kN]	$\omega_{u,\#S}$ [mm]	$N_{u,exp}$ [kN]	$\omega_{u,exp}$ [mm]
88.9×2.6-400-P	0.22	3	382.8	1.59	399.2	0.30	425.2	2.91
88.9×2.6-550-P	0.30	3	370.9	1.25	392.7	0.27	404.6	2.60
88.9×2.6-750-P	0.41	3	361.6	2.08	368.0	1.30	389.6	2.75
88.9×2.6-950-P	0.51	3	333.4	3.82	337.2	2.43	344.4	4.54
88.9×2.6-1150-P	0.62	3	306.9	5.88	301.9	3.03	295.3	8.09
88.9×2.6-1650-P	0.89	3	232.4	12.03	243.8	12.40	243.4	10.32
88.9×2.6-2150-P	1.15	4	168.9	17.60	178.7	17.51	164.7	19.79
88.9×2.6-2650-P	1.42	4	134.0	20.95	142.0	17.31	126.4	20.63
88.9×2.6-3080-P	1.65	4	106.5	26.39	114.3	24.98	100.5	25.81

Table 4: Statistical somparison of the model approaches #A (ANSYS) and #S (SCIA Engineer)

Item	#A (ANSYS)	#S (SCIA Engineer)
Mean (average) $N_{u,\#}/N_{u,exp}$ [-]	0.984	1.023
Standard deviation $N_{u,\#}/N_{u,exp}$ [-]	0.060	0.071
Coefficient of variation (CoV) $N_{u,\#}/N_{u,exp}$ [%]	6.06	6.95
Mean (average) $\omega_{u,\#}/\ \omega_{u,exp}$ [-]	0.827	0.609
Standard deviation $\omega_{u,\#}/\ \omega_{u,exp}$ [-]	0.212	0.365
Coefficient of variation (CoV) $\omega_{u,\#}/\ \omega_{u,exp}$ [%]	25.65	59.92

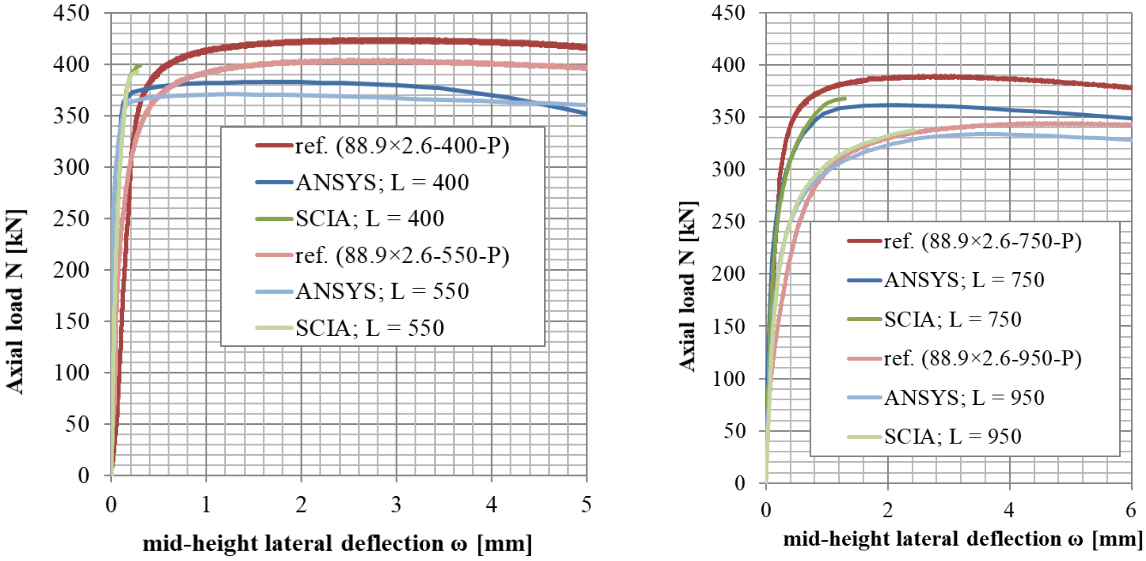

(a) (b)

Figure 4: Experimental and FE axial loads (N) vs. mid-height lateral deflection (ω) curves

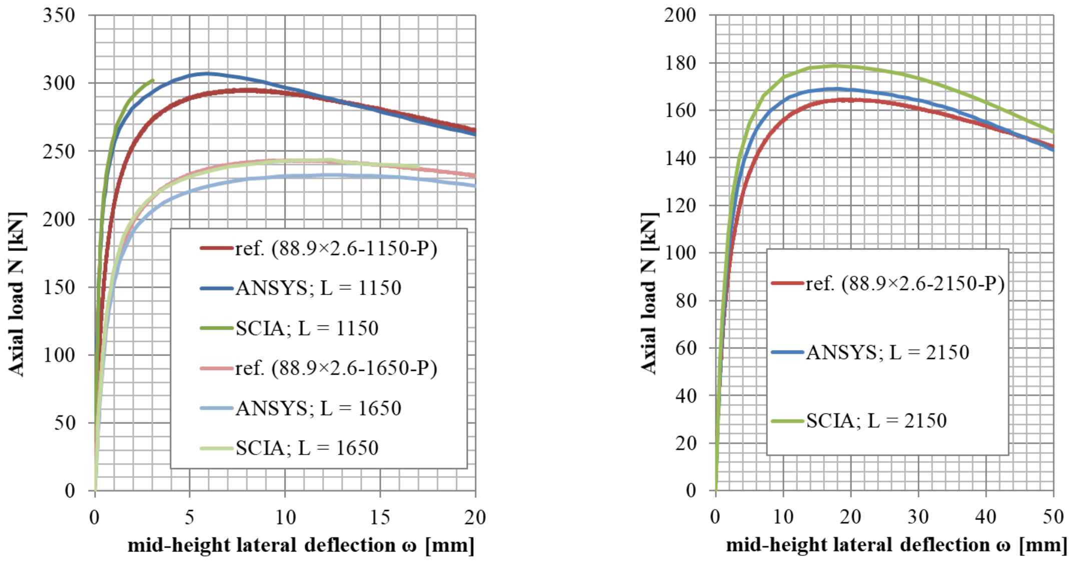

(a) (b)

Figure 5: Experimental and FE axial loads (N) vs. mid-height lateral deflection (ω) curves

Multilinear material model has been considered for the cases depicted in the Figure 4, Figure 5 and the Figure 6 a. The comparison of the results, where either multilinear or bilinear material model has been utilized is documented for the longest specimen (structural length of 3080 mm) in the Figure 6 b.

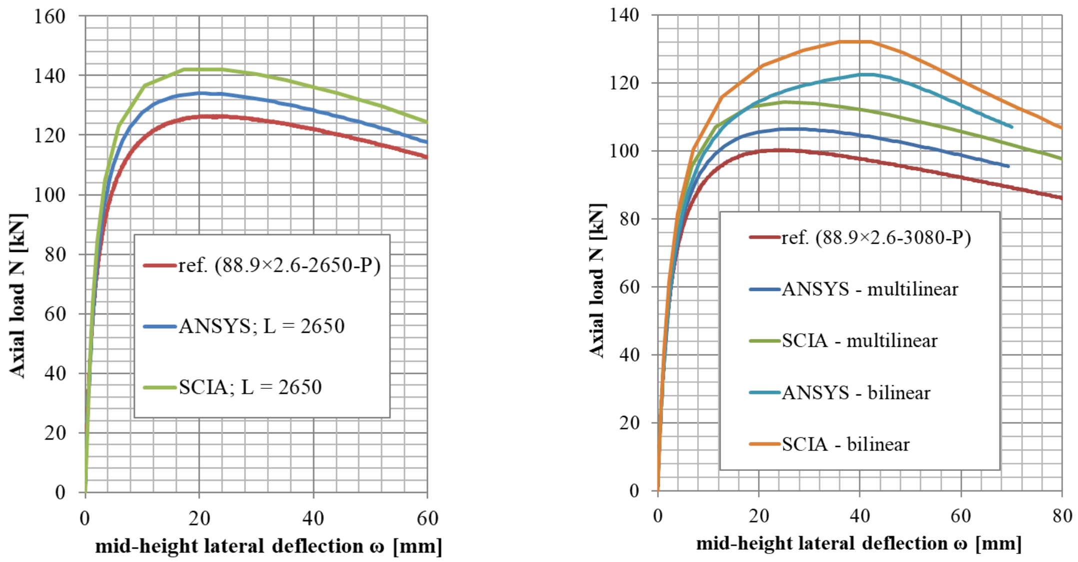

(a) (b)

Figure 6: Experimental and FE axial loads (N) vs. mid-height lateral deflection (ω) curves

5 DISCUSSION

Global buckling was the most common failure mode. In case of the shortest specimens, a local buckle has developed in the area near the mid-height of the more compressed side of the tubular cross-section, at the moment of the peak load. Obtained buckling shapes are comparable to those presented in the study by Mr. Buchanan et al. [5].

The comparison of the results obtained from two different solvers, ANSYS (approach #A) and SCIA Engineer (approach #S) is performed utilizing the normalized values of the axial load $N_{u,\#}/N_{u,exp}$ and the normalized value of the mid-height lateral deflection $\omega_{u,\#}/\omega_{u,exp}$. Average (mean) values, standard deviations and CoV (coefficient of variation) are tabulated in Table 4, and also illustrated graphically in the Figure 7 (average values along with the standard deviation bars). Only the results of the numerical models utilizing the multilinear material model description have been considered for the statistical evaluation. It is obvious, that the simplification in the material model by adopting the bilinear stress-strain description (Figure 6 b) has not yield appropriate results.

In case of the normalized ultimate axial load, $N_{u,\#}/N_{u,exp}$, both solvers resulted in practically the same average values, very close to 1.0, with the coefficient of variation (CoV) equal to 6 and 7 % for the approaches #A and #S respectively.

For the normalized ultimate mid-height lateral deflection $\omega_{u,\#}/\omega_{u,exp}$, the average value of the approach #A has resulted in the value of 0.83 (much closer to 1.0, with the CoV of 26%), whereas for the approach #S in value of 0.61 (with the CoV of 60%). The reason of this is rather flat nature of the load-deflection curve in the area around its peak, and the step-size sensitivity of the nonlinear analysis at this stage. For the shorter specimens (Figure 4 and Figure 5 a), the last converged sub steps of the nonlinear numerical analyses (for approaches #S - SCIA) are rather far from the peak value in the matter of deflection (flat nature of the curves). At this stages, the numerical analyses are rather sensitive of the step size. The environment of SCIA Engineer does not support yet such robustness in the step-size alternation as the environment of ANSYS Classic. In SCIA Engineer, the alternation of the step size of the analysis is possible at the initiation of the process only. However, in ANSYS, the alternation of the step size available also during the analysis process makes the process much more feasible. Moreover, the post processing environment of SCIA Engineer for the geometrically nonlinear analyses is not yet developed as much in order to feasibly monitor the data from every sub step of the nonlinear analyses. Therefore, the step size during the nonlinear analysis in SCIA was not set up as sufficiently small at the stage it was required to be small (near the peak load).

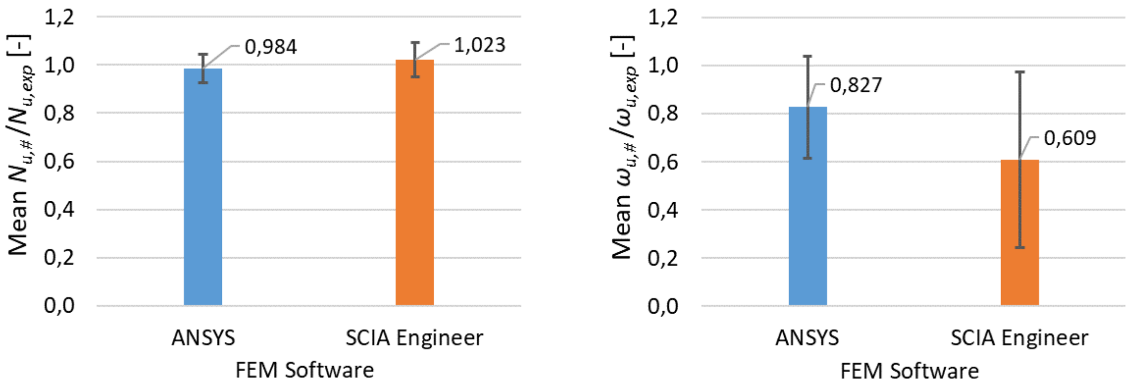

(a) (b)

Figure 7: Graphical depiction of the statistical parameters

In case it would be feasible to conduct and monitor the results of the analyses documented in the Figure 4 and Figure 5 a in SCIA Engineer software further (to better capture the area around the load-deflection curve peak), it is very likely the average value of the normalized ultimate mid-height lateral deflections $\omega_{u,\#}/\omega_{u,exp}$ (Figure 7 b) would result in much better value (closer to 1.0), and with much smaller coefficient of variation (CoV), similar to the values obtained from ANSYS (Table 4).

6 CONCLUSIONS

The advanced numerical simulation processes of duplex stainless steel circular hollow section columns have been conducted utilizing ANSYS solver (approach #A) and the FEM solver implemented in SCIA Engineer software (approach #S). Geometrically nonlinear analyses of 9 columns of various lengths and the same cross section (88.9×2.6 CHS) exposed to compressive loading including the global geometrical imperfections have been conducted.

The application of the simplified bilinear material model for the stainless steel material has not resulted in the load-deflection response which would be in a nice match with the experimental data (Figure 6 b). In order to model the behavior of the stainless steel structural elements properly, the multilinear stress-strain dependence in accordance with the Ramberg and Osgood relations is essential to be utilized.

The difference between the average values of the normalized ultimate axial load $N_{u,\#}/N_{u,exp}$ obtained either by the approach #A (ANSYS) or #S (SCIA Engineer) is rather negligible. For both cases, the average value was very close to 1.0, with the coefficient of variation 6-7%.

However, for the normalized ultimate mid-height lateral deflection $\omega_{u,\#}/\omega_{u,exp}$, the average values are 0.83 and 0.61, with CoV 26% and 60% for the approach #A and #S respectively. These numbers are caused by flat nature of the load-deflection curve in the area of its peak value. Moreover, in case of the numerical analyses conducted in SCIA Engineer (approach #S), the sub step size during the nonlinear analyses was not set up as sufficiently small to obtain better results. The reason of this is not yet developed post processing environment of SCIA Engineer in order to process the results of geometrically nonlinear analyses in detail.

SCIA Engineer software focuses rather on conventional civil engineering applications, as are designs and checks of structures in accordance with various standards, as these features are much more demanded in the market of the civil engineering structural design. ANSYS on the other hand is a tool which enables almost any kind of analysis, but does not offer any designs or checks of structural components according to standards, and therefore would not be so comfortable and easy to use for the majority of the civil engineering applications. However, it was found that the FEM solver of SCIA Engineer has a capacity to conduct proper materially and geometrically nonlinear analyses including initial geometrical imperfections. The only obstacle is the post processing for such process, which of course could be developed in case of customer demand.

ACKNOWLEDGEMENT(S)

This paper has been created with the financial support of the Czech Science Foundation by project No.: 20−00761S "Influence of material properties of stainless steels on the reliability of bridge structures". Additional financial support was provided by the BUT fund for specific university research, project number FAST-J-21-7169.

We would like to gratefully thank Mr. Craig Buchanan, Mr. Leroy Gardner, and Mrs. Esther Real for sharing the processed data curves of their conducted experiment.

REFERENCES

[1] Baddoo, N.R. Stainless steel in construction: A review of research, applications, challenges and opportunities. *J. Constr. Steel Res.* (2008) **64**(11): p.1199–1206. ISSN: 0143-974X. doi:10.1016/j.jcsr.2008.07.011.

[2] Sobrino, J.A; Stainless Steel Road Bridge in Menorca, Spain. *Structural Engineering international*. IABSE, (2006) **16**(2): p. 96-100, ISSN: 1016–8664.

[3] Ramberg, W., Osgood, W.R. Description of stress-strain curves by three parameters. Technical Note No. 902. National Advisory Committee for Aeronautics, Washington D.C (1943).

[4] Hill, H.N. Determination of stress-strain relations from the offset yield strength values. Technical Note No. 927. National Advisory Committee for Aeronautics, Washington D.C. (1944).

[5] Buchanan, D., Real, E., Gardner, L. Testing, simulation and design of cold-formed stainless steel CHS columns. *Thin-Walled Struct.* (2018) **130**: p.297-312. ISSN: 0263–8231. doi:10.1016/j.tws.2018.05.006.

[6] Dassault Systèmes Simulia Corp. Abaqus/CAE 2016 (2015).

[7] Gardner, L., Nethercot, D.A. Experiments on stainless steel hollow sections - Part 1:

Material and cross-sectional behaviour. *J. Constr. Steel Res.* (2004) **60**: p. 1291–1318. doi:10.1016/j.jcsr.2003.11.006.
[8] Buchanan, D., Zhao, O., Real, E., Gardner, L. Cold-formed stainless steel CHS beam-columns - Testing, simulation and design. *Eng. Struct.* (2020) **213**. ISSN: 0141–0296. doi:10.1016/j.engstruct.2020.110270.
[9] Arrayago, I., Rasmussen, K.J.R., Real, E. Statistical analysis of the material, geometrical and imperfection characteristics of structural stainless steels and members. *J. Constr. Steel Res.* (2020) **175**, ISSN: 0143-974X. doi:10.1016/j.jcsr.2020.106378.
[10] Ansys, Inc. ANSYS 19.0. Canonsburg, PA 15317 U.S.A. (2018)**.**
[11] Nemetschek Group. SCIA Engineer 20.0. Hasselt 3500 Belgium (2020).
[12] Jindra, D., Kala, Z., Kala, J., Validation of Stainless-Steel CHS Columns Finite Element Models. *Materials* (2021) **14**(7) doi: 10.3390/ma14071785.
[13] Kala, Z., Valeš, J., Jonsson, J., Random fields of initial out of straightness leading to column buckling. *J. Civ. Eng. Man.* (2017) **23**(7) ISSN: 1392–3730. doi: 10.3846/13923730.2017.1341957.
[14] Shayan, A., Rasmussen, J.R., Zhang, H., On the modelling of initial geometric imperfections of steel frames in advanced analysis. *J. Constr. Steel Res.* (2014) **98**: p. 167–177. ISSN: 0143-974X. doi: 10.1016/j.jcsr.2014.02.016.
[15] Gardner, L., Nethercot, D.A., Numerical modelling of cold-formed stainless steel sections, In: Mäkeläinen, et al., editors. Proceedings of the 9th Nordic Steel Construction Conference, Helsinki, Finland, (2001) p. 781–789.
[16] Mirambell, E., Real, E., On the calculation of deflections in structural stainless steel beams: an experimental and numerical investigation. *J. Constr. Steel Res*. (2000) **54**: p. 109–133.
[17] Jindra, D., Kala, Z., Seitl, S., Kala, J, Material model parameter identification of stainless steel (AISI 304L). *26th International Conference Engineering Mechanics 2020,* (2020) p. 246–249.
[18] Cruise, R.B.; Gardner L.; Residual stress analysis of structural stainless steel sections. *J. Constr. Steel Res.* (2008) **64**(3): p. 352–366. doi:10.1016/j.jcsr.2007.08.001.
[19] Jandera, M., Gardner, L., Machacek, J., Residual stresses in cold-rolled stainless steel hollow sections. *J. Constr. Steel Res.* (2008) **64**(11): p. 1255–1263. doi:10.1016/j.jcsr.2008.07.022.
[20] European Committee for Standardization. EN 1993-1-4:2006+A1:2015 Eurocode 3 - design of Steel Structures - Part 1-4: General rules - Supplementary rules for Stainless Steels. Brussels, Belgium (2015).